Effect of Reconstruction and Filtering on Kinetic Parameter Estimation Bias and Reliability for Dynamic SPECT: A Simulation Study

Lingfeng Wen, *Student Member, IEEE*, Stefan Eberl, *Member, IEEE*, Koon-Pong Wong, *Member, IEEE*, Dagan Feng, *Fellow, IEEE*, and Jing Bai, *Fellow, IEEE*

***Abstract*—Dynamic SPECT has the potential to provide absolute physiological parameter estimates. However, the low sensitivity of SPECT typically results in very noisy dynamic SPECT data. Filtering can reduce the noise, but at the expense of degrading the already poor resolution further. The effect of reconstruction parameters, post-reconstruction filtering and resolution recovery on kinetic parameter estimation bias and reliability was systematically investigated. Dynamic projection data were generated using Monte Carlo (MC) simulations of a mathematical brain phantom at 10 different levels of Poisson noise. The projection data were reconstructed with OSEM with varying numbers of iterations and subsets and were filtered with three-dimensional (3-D) Gaussian filters with varying FWHM. Bias and reliability of the main parameters of interest (K_1, V_d, and binding potential) for thalamus, cerebellum, and frontal cortex were estimated for the three-compartment model fits to the tissue time-activity curves derived from the reconstructed data. Reliability (standard deviation) of parameter estimates was obtained with the Bootstrap MC technique, which showed good agreement with conventional MC in a subset of data sets, but required only a small fraction of conventional MC computation time. Post-reconstruction filtering increased bias, without improving the reliability of parameter estimates and, hence, no post-reconstruction filtering is recommended. For reconstructions without resolution recovery, an effective number of 40 iterations overall provided the best tradeoff between bias and reliability for the range of noise levels studied. Resolution recovery achieved a modest reduction in bias.**

***Index Terms*—Filtering, image reconstruction, Monte Carlo methods, quantitative analysis, single photon emission computed tomography.**

I. Introduction

With the more widespread availability of multidetector single photon emission computed tomography (SPECT) systems and advances in attenuation and scatter correction, estimation of regional physiological kinetic rates has become feasible with quantitative dynamic SPECT [1], [2]. The kinetic parameters, describing the biological and physiological process of interest, are typically estimated by fitting compartment models to curves derived from quantitative dynamic SPECT studies. Even with the improved sensitivity of multidetector systems, the sensitivity of SPECT is still at least an order of magnitude lower than that achievable with Positron Emission Tomography (PET), resulting in a high level of image noise at the short dynamic frame times required for kinetic modeling, which can affect the reliability of the parameter estimates. In addition, the resolution of SPECT is relatively poor, leading to biased estimates due to partial volume effects.

The most frequently used reconstruction algorithm in clinical SPECT is still filtered backprojection (FBP). FBP is attractive due to its high speed, but potentially suffers from streak artifacts [3] and absolute quantification is difficult to achieve with FBP. Iterative algorithms can offer improved reconstructed image quality and quantitative accuracy [4]. Their main disadvantage of long reconstruction times has largely been overcome with the introduction of faster computers and accelerated algorithms. Maximum likelihood estimation with expectation maximization (ML-EM) is an efficient iterative reconstruction method for SPECT [5] and can take into account many physical processes, such as nonuniform attenuation, scatter effect, and noise properties [6]–[9]. Several methods have been proposed to speed up the algorithms. The Ordered Subsets Expectation Maximization (OS-EM) proposed in [10] has been shown to share the desirable properties of ML-EM, especially predictability and nonnegativity [11], while accelerating reconstruction time by a factor close to the number of subsets used [12].

In SPECT, some form of low-pass filtering is typically applied to reduce noise and aid in the visual interpretation of the images [3]. Filtering can be applied pre-, during, and post-reconstruction. While various filters can be used for SPECT reconstruction [13]–[15], the three-dimensional (3-D) Gaussian filter is attractive for quantitative studies as it does not introduce negative values and maintains quantitative accuracy [16], [17] and thus was selected for this study.

Filtering reduces noise and, hence, may improve the reliability of the estimated kinetic parameters, whereas it further degrades the already poor resolution and accentuates partial volume effects and may thus have an adverse affect on parameter estimate bias. While the effect of post-reconstruction filtering on image quality has been investigated [18], [19],

Manuscript received July 4, 2003; revised August 31, 2004. This work was supported in part by grants from the ARC, RGC, and NSFC.

L. Wen is with the Department of Biomedical Engineering, Tsinghua University, Beijing 100084, China. He is also with the School of Information Technologies, University of Sydney, NSW 2006, Australia (e-mail: wenlf@ieee.org).

S. Eberl is with the Department of PET and Nuclear Medicine, Royal Prince Alfred Hospital, Sydney, NSW 2050, Australia. He is also with the School of Information Technologies, University of Sydney, NSW 2006, Australia (e-mail: stefan@cs.usyd.edu.au).

K.-P. Wong and D. Feng are with the School of Information Technologies, University of Sydney, NSW 2006, Australia. They are also with the Center for Multimedia Signal Processing, Department of Electronic and Information Engineering, Hong Kong Polytechnic University, Hong Kong (e-mail: wong.kp@polyu.edu.hk; feng@cs.usyd.edu.au).

J. Bai is with the Department of Biomedical Engineering, Tsinghua University, Beijing 100084, China (e-mail: deabj@tsinghua.edu.cn).

Digital Object Identifier 10.1109/TNS.2005.843622

these studies did not take into account the quantitative information for dynamic SPECT. The objective of this study thus was to evaluate the effect of post-reconstruction filtering and reconstruction parameters (number of iterations and subsets for OS-EM) on kinetic parameter estimation bias and reliability for dynamic SPECT in the human brain. Furthermore, investigation into the tradeoff between post-reconstruction filtering and reconstruction parameters was also performed.

II. Methods

A. 3-D Brain Phantom

Simulations were based on a mathematical brain phantom based on the Zubal anatomical phantom [20]. The phantom was derived from MRI data and anatomical structures within the brain were identified by index number in the $256 \times 256 \times 128$ volume covering the brain.

B. Projection Data Acquisition

Projection data were generated with the SimSET Monte Carlo code [21]. A parallel hole collimator and an energy window of 20% centered around 159 keV for ^{123}I were assumed. The detector module specified a simple Gaussian energy blurring model for a flat SPECT detector with an energy resolution of 10% full-width at half maximum (FWHM). Scatter and photon attenuation effects were included in the simulations. The simulated data were binned into 120 projections over the 360° rotation. Matrix size used for each projection was 128×85 (pixel size 2.344 mm $\times$ 2.353 mm).

To allow different kinetics to be assigned to different brain structures, each of the individual brain structures, identified in Table I, were simulated in isolation (activity in all other structures set to zero) for a total number of five hundred million decays each. This provided low-noise projection data sets for each identified structure. Projections for total brain activity could then be generated by weighted sum of the projections for the individual structures.

C. Dynamic Projection Data With Poisson Noise

To simulate the dynamic data set, the tissue time-activity curves (TTAC) (see Fig. 1) were generated from the estimated rate constants and plasma time-activity curve (PTAC) determined in baboon experiments of the neuronal nicotinic acetylcholine receptor tracer 5-[^{123}I]-iodo-A-85 380 [22], [23]. The composite sets of dynamic projections for all brain structures were generated by multiplying the projections of individual structures with the corresponding values from TTACs at the selected time points. The final dynamic projection set consisted of fifteen 60 s scans, nine 300 s scans and twelve 600 s scans for a total collection time of 3 h. The composite dynamic projection data were then scaled to appropriate pixel counts typical of those observed with the tracer in the experimental study to allow adding realistic noise levels. The maximum pixel count for a 5 min frame near peak uptake in the brain was found to be about 30 counts/pixel. A scaling factor was thus determined to give a maximum pixel count of 30 counts per pixel for a similar 5 min frame in the simulated composite dynamic projection and the whole dynamic projection data set was scaled by the scaling factor. Frames with collection times other than 5 min were further scaled based on the relative collection time (i.e., divided by 5 for 1 min frames). Poisson noise was then added to the scaled projections and the noisy projections were normalized to represent counts per minute. The same procedure was utilized to generate noisy projections simulating maximum 5 min frame pixel counts which ranged from 10 to 50, to allow evaluation for different noise levels. Low-noise projections were also generated using the same method, but without adding Poisson noise.

TABLE I
The Simulated Brain Structures and Corresponding Tissue Time-Activity Curves

Individual brain structure simulated	Number of voxels	TTAC used for the structure
thalamus	7308	thalamus
frontal lobes	69331	frontal cortex
cerebellum	86964	cerebellum
pons	13515	frontal cortex
occipital lobes	43108	frontal cortex
hippocampus	4275	frontal cortex
caudate nucleus	6078	frontal cortex
insula cortex	8019	frontal cortex
putamen	5873	frontal cortex
special region frontal lobes	3539	frontal cortex
temporal lobes	141570	frontal cortex
amygdala	2364	frontal cortex
white matter [a]	299721	
optic nerve [a]	767	
internal capsule [a]	5347	white matter
septum pellucidum [a]	597	
corpus callosum [a]	6651	

[a] These structures were simulated together into one composite projection.

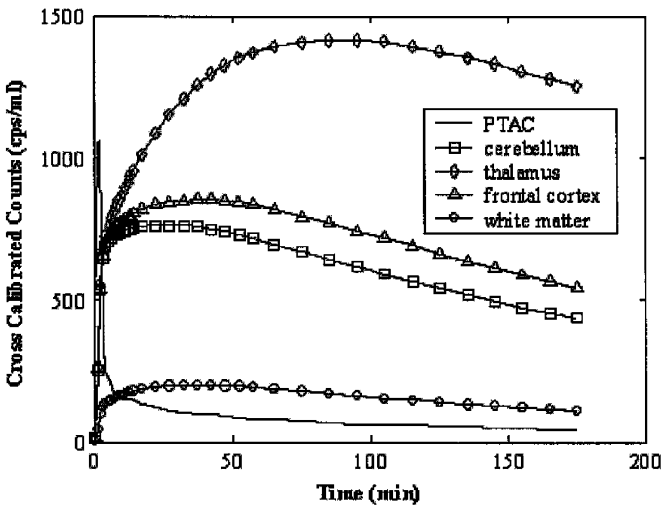

Fig. 1. Plots of plasma time-activity curve and tissue time-activity curves for the frontal cortex, thalamus, cerebellum, and white matter.

D. Reconstruction and Post-Reconstruction Filtering

Emission projections were reconstructed using the OS-EM iterative reconstruction algorithm with varying number of iterations and different numbers of subsets [10]. The number of subsets used was 5, 10, 20, 30, 40, and 60, while the number of iterations ranged from 1 to 8. Attenuation was corrected with the attenuation maps derived from the mathematical brain phantom and attenuation coefficients appropriate for ^{123}I [22]. Compensations for the effect of scatter and the detector-collimator response functions were not applied. The reconstructed slices were stored in $128 \times 128 \times 85$ data volumes with voxel sizes of $2.344 \times 2.344 \times 2.353$ mm. Finally, 3-D Gaussian filters were applied to smooth the reconstructed images with the FWHM ranging from 3 to 8 pixels (7 to 19 mm). Data without any post-reconstruction filtering $(\mathrm{FWHM} = 0)$ were also included in the analysis.

The limited resolution of SPECT imaging can be included in the imaging model of OS-EM reconstruction to achieve resolution recovery and potentially reduce bias due to partial volume effects. Reconstructions were also performed with resolution recovery, using the known resolution degradation from the Monte Carlo simulations. Due to the slower convergence with resolution recovery, reconstructions with 40 subsets and 10 iterations, 40 subsets and 20 iterations were performed. TTACs were generated and fitted as for the reconstructions without resolution recovery. As the aim of resolution recovery was to optimize resolution and minimize bias, no post reconstruction filtering was performed for these reconstructions.

E. Kinetic Analysis

Tight volumes of interest (VOIs) for frontal cortex, thalamus, and cerebellum were derived by eroding the definition of the structure in the mathematical brain phantom with 2, 3, and 5 pixel wide masks for frontal cortex, thalamus and cerebellum, respectively. TTACs generated for each VOI were fitted to a three-compartment (two tissue compartments) model, using nonlinear least squares curve fitting with Marquardt-Levenberg minimization [24]. The PTAC was scaled in the same fashion as the projection data and is also shown in Fig. 1. A modified cost function was used in the fitting based on integrating the count rates over the frame duration [25], [26].

Parameters of primary interest for this tracer were the influx rate constant K_1, the volume of distribution V_d (1), the binding potentials BP_1 (2) [27], and BP_2 defined by (3) [28]

$$V_d = K_1(k_3 + k_4)/(k_2 k_4) \tag{1}$$

$$BP_1 = k_3/k_4 \tag{2}$$

$$BP_2 = K_1 k_3/(k_2 k_4). \tag{3}$$

To ensure successful fits to the three-compartment model, the following strategy was used. The data were first fitted with a two-compartment model, and the initial conditions for the three-compartment model fit were derived from the fitted parameters of the two-compartment model fit. If the three-compartment model fit gave a V_d which was greater than twice that of the two-compartment model fit, or if the residual sums of square (RSSQ) of three compartment fit was greater than $1.1 \times \mathrm{RSSQ}$ of the two-compartment model fit, the fit of the three-compartment model fit was repeated with a different random perturbation of the initial conditions so as to eliminate poor fits to the data and clearly nonphysiological V_d values.

TABLE II
THE REFERENCE PARAMETER SETS FOR THE VOLUMES OF INTERESTS

Cortex	K_1	k_2	k_3	k_4	V_d	BP_1	BP_2
cerebellum	0.275	0.063	0.029	0.035	7.938	0.821	3.566
frontal cortex	0.277	0.059	0.038	0.037	9.628	1.038	4.870
thalamus	0.285	0.061	0.144	0.041	21.512	3.594	16.673
white matter [a]	0.05	0.025					

[a] Two-compartment and two-parameter model fit

The "bootstrap" Monte Carlo technique with 100 iterations was used to determine the standard deviations (SD) and coefficients of variation (CV) of the parameters of interest. Given a curve of n data points, for each bootstrap Monte Carlo iteration, n points are randomly selected from the curve and the model fitted to the n randomly selected points. As each point is obtained by randomly drawing from the curve of n points, some of the points from the original data set will be used more than once for a particular realization, while others will not be used. The points which are duplicated and not selected will vary randomly for each iteration. For the 36 point TTACs used in this study an example of a sample of randomly drawn points for one realization is using points (sorted in ascending order) [1, 1, 2, 4, 6, 6, 6, 11, 12, 13, 13, 16, 17, 18, 18, 18, 19, 21, 21, 21, 21, 22, 23, 23, 24, 26, 26, 28, 28, 30, 31, 34, 34, 34, 36]. For this particular realization, point 1 is used twice, point 3 is not used at all and point 21 is used 4 times etc. In this way, 100 "bootstrap" TTACs were generated for each noise level and cortex region.

F. Evaluation

Bias was calculated by comparing the mean fitted parameters from the 100 bootstrap Monte Carlo iterations with the known parameters (see Table II) for the TTACs (see Fig. 1) used for generating the dynamic projection. Parameter estimate CV was calculated from the standard deviation derived from the bootstrap Monte Carlo iterations, and then divided by the known parameters listed in Table II.

Graphs of percentage bias vs. CV were plotted for the parameters of interests and for all noise levels and structures for the different reconstruction and filtering parameters. The points then represent the effect of reconstruction parameters and post-reconstruction filtering on bias and reliability of the estimated parameters (see Fig. 2). A region was identified manually on the graph, which provided the best tradeoff between reliability and bias (elliptical region on Fig. 2), i.e., achieved the best compromise between bias and CV. As shown in Fig. 2, points with low bias and slightly elevated, but acceptable CV $(<10\%)$ also included in the region, as these points were also considered acceptable from the point of view of bias versus CV tradeoff. However, the point with clearly elevated CV $(>13\%)$, but low bias was excluded.

If a particular combination of subset, iteration, and filtering produces a bias/CV point within the identified region, then it

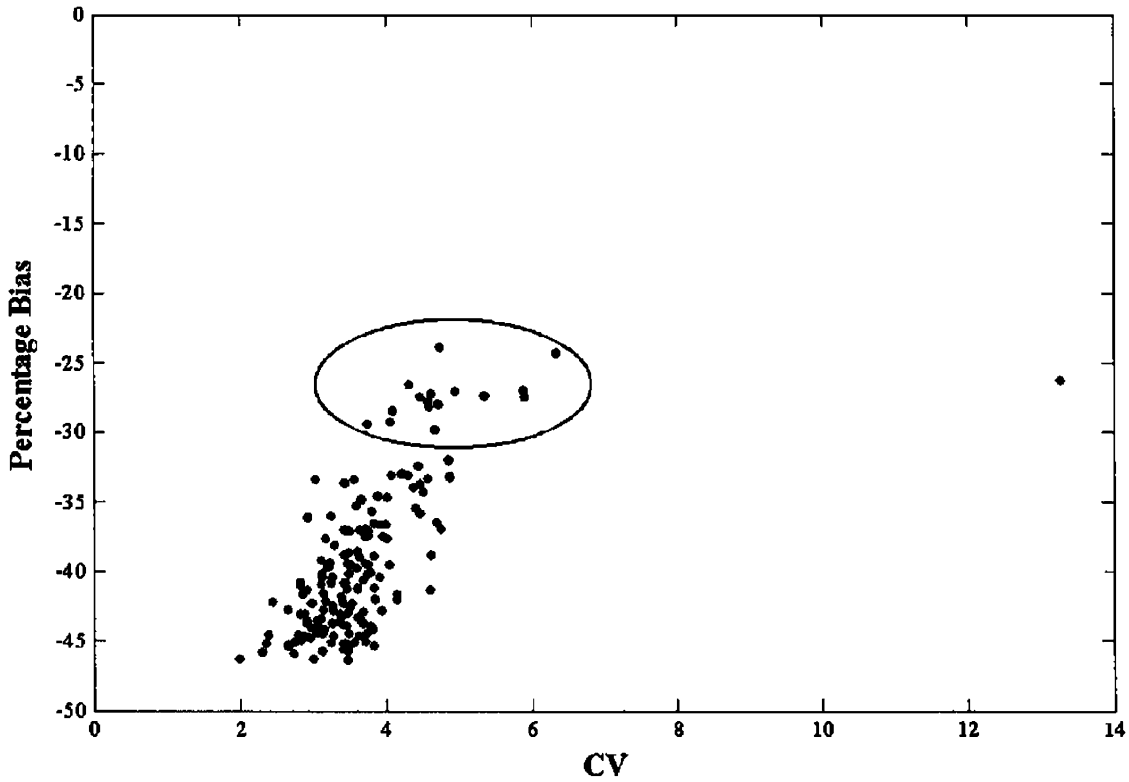

Fig. 2. Plot of %-bias versus CV for K_1 in the cerebellum for the noise level 30 data. Curve points representing best compromise between bias and reliability are enclosed by an ellipse and the corresponding reconstruction and filter parameters received a score of 1. All others received a score of zero for this parameter (K_1) and region (cerebellum).

received a score of 1, otherwise a score of 0. The scores for all data sets (different noise levels and brain structures) were then summed to provide an overall score for each combination of subset, iteration, and filtering.

G. Comparison Between Conventional and Bootstrap Monte Carlo Simulations

As indicated above, the Bootstrap Monte Carlo technique was used to estimate the SD and CV associated with the estimated parameters to demonstrate the effects of noise and filtering on the parameter estimation reliability. The main advantage of the Bootstrap Monte Carlo technique over conventional Monte Carlo in this application is a substantial reduction in the number of reconstructions. For the 10 noise levels, 36 frames per dynamic study and 24 different reconstruction parameters, Bootstrap Monte Carlo required 8640 sets of projections to be reconstructed. Assuming 100 iterations, conventional Monte Carlo technique generating a different set of projection for each iteration would have required 864 000 sets of projections to be reconstructed which is associated with an almost prohibitive computation time.

To compare Bootstrap Monte Carlo Estimation of SD and CV with conventional Monte Carlo estimation, 100 iterations of conventional Monte Carlo simulations were generated for all noise levels and one set of reconstruction parameters (20 subsets and two iterations). TTACs were then generated for each of the reconstructed sets of data and fitted with the compartmental model as described above. The SDs and CVs were calculated from the fits to the 100 iterations. These were then compared with the Bootstrap Monte Carlo estimates of CV and SD.

III. Results

A. Percentage Bias and CV

Successful reconstructions and curve fits were obtained for noise free and the nine noise levels based on the maximum pixel values for 5 min frame of 10, 15, 20, 25, 30, 35, 40, 45, and 50. Fig. 3 shows curves of percentage bias and CV for K_1 and V_d over the range of noise levels studied as a function of post-reconstruction filter FWHM for a reconstruction using 20 subsets and two iterations for the thalamus. Little systematic improvement in CV was observed with increasing filter FWHM and this was also observed for the cerebellum and frontal cortex regions. The CVs of K_1 were below 5% for all selected regions and noise levels and those for V_d were less than 1.5%. Filtering did not improve the reliability, whereas increasing FWHM increased the bias of K_1 and V_d estimates. A similar trend in bias with increasing FWHM was also observed in the cerebellum and frontal cortex. Compared with the thalamus, bias in the frontal cortex was more pronounced (for noise30, K_1 bias of -43.1% and -60.4% for FWHM of 0 and 8 pixels, respectively and V_d bias of -44.1% and -59.9% for FWHM of 0 and 8 pixels, respectively) and not unexpectedly, less in the larger cerebellum region (for noise30, K_1 bias of -5.2% and -23.4% for FWHM of 0 and 8 pixels, respectively and V_d bias of -5.0% and -21.9% for FWHM of 0 and 8 pixels, respectively).

Similar graphs for bias and CV are shown for BP_1 and BP_2 in Fig. 4 for the thalamus. The findings for BP_2 were similar to those for K_1 and V_d. BP_1 for the thalamus showed only moderate increase in bias with increasing filter FWHM, as well as showing some improvement in CV with a moderate amount

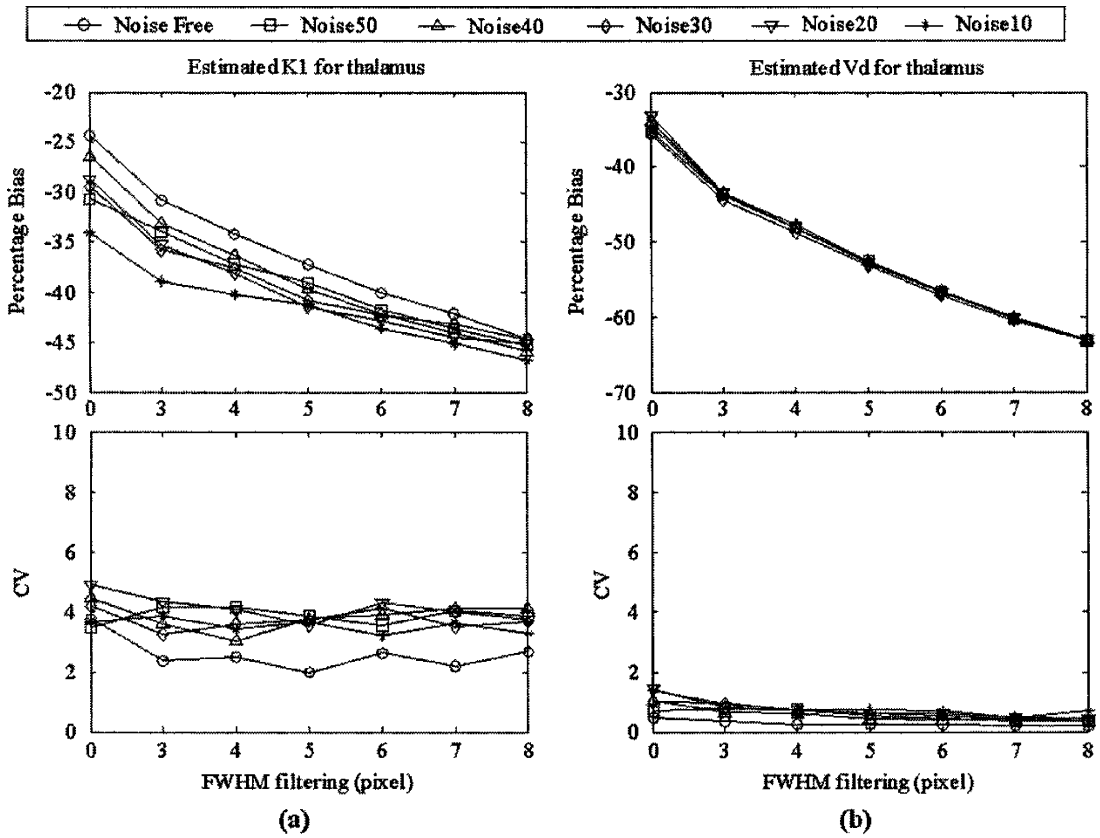

Fig. 3. Percentage bias (top) and CV (bottom) of estimated (a) K_1 and (b) V_d for the thalamus as a function of filter FWHM. Data were reconstructed with 20 subsets and two iterations.

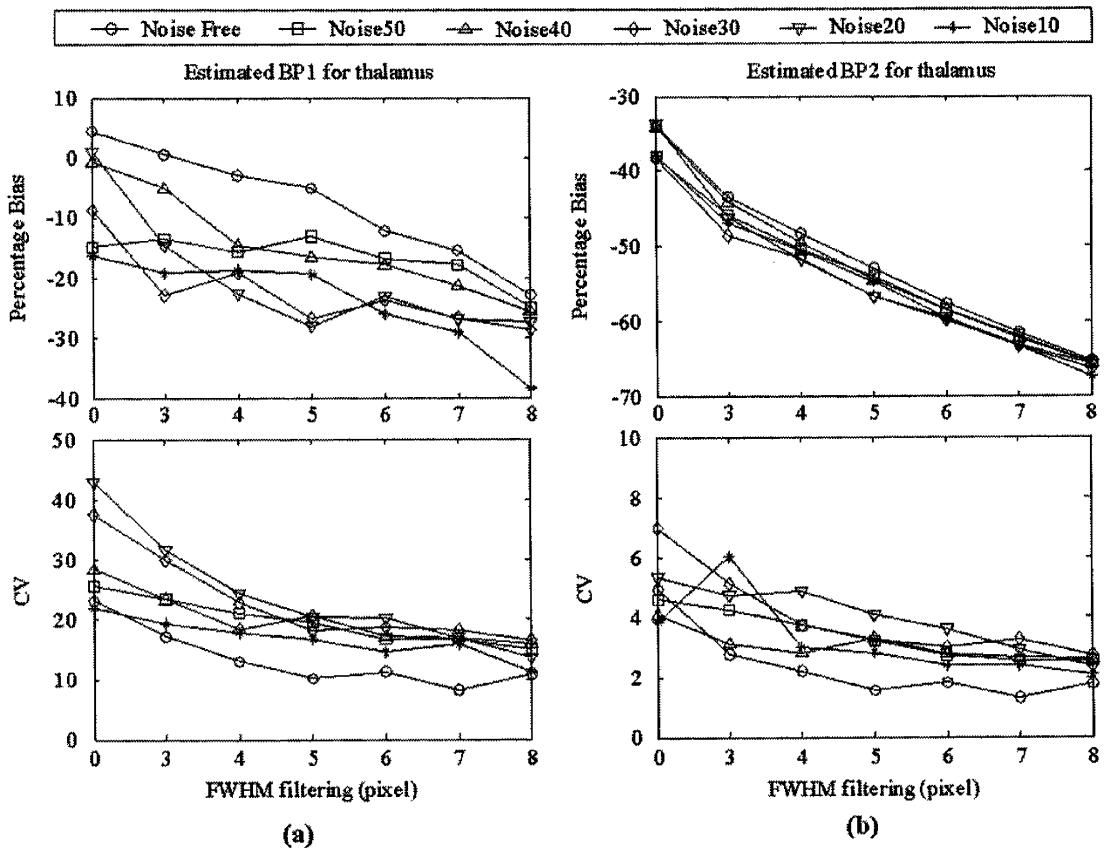

Fig. 4. Percentage bias (top) and CV (bottom) of estimated (a) BP_1 and (b) BP_2 for the thalamus as a function of filter FWHM. Data were reconstructed with 20 subsets and two iterations.

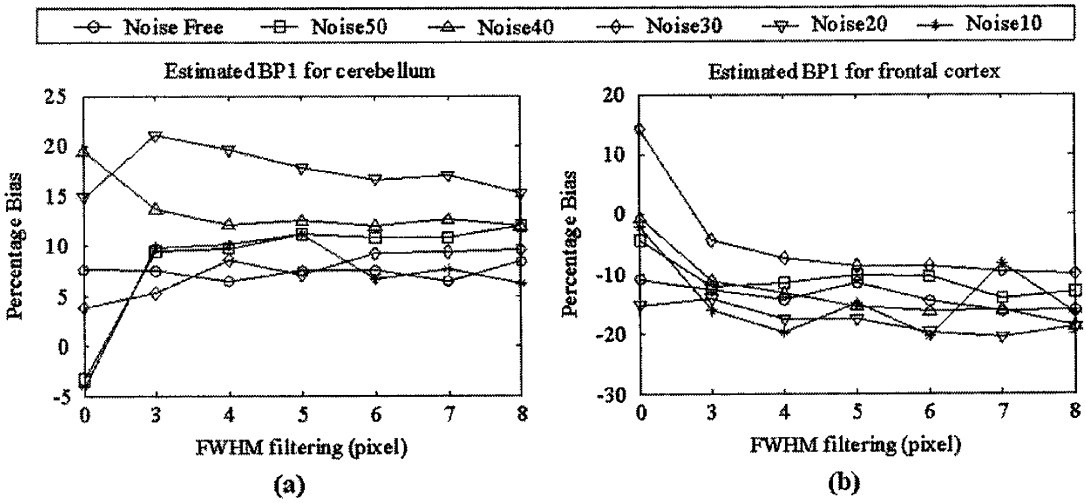

Fig. 5. Percentage bias of estimated BP_1 for (a) the cerebellum and (b) the frontal cortex.

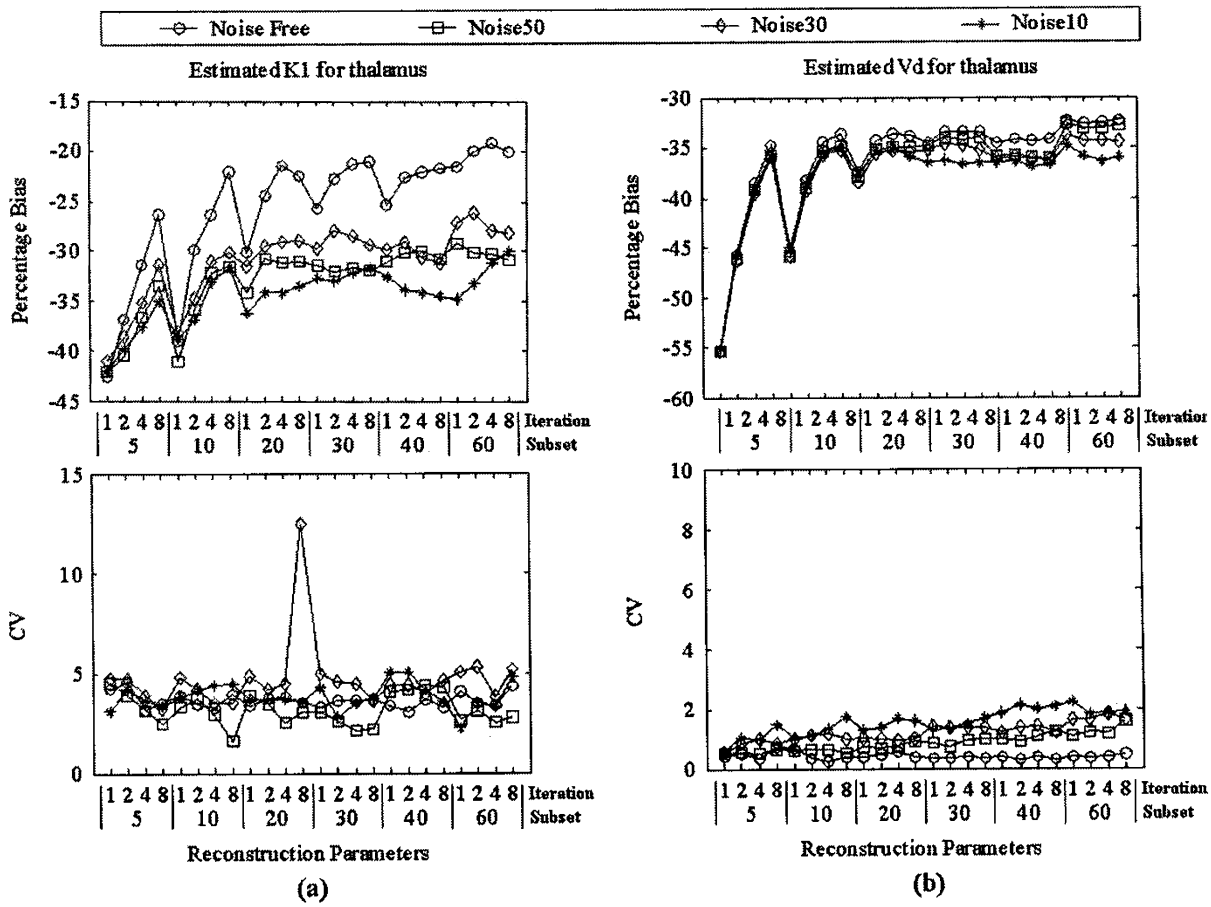

Fig. 6. Plots of %-bias and CV as a function of reconstruction parameters (number of subsets: number of iterations). Results are for reconstructions without any post-reconstruction filtering.

of filtering. Percentage bias graphs for BP_1 in the cerebellum and frontal cortex are shown in Fig. 5. These regions did not show the pronounced bias and bias was relatively constant as a function of filter FWHM. Again reliability improved moderately for a limited amount of filtering (FWHM $= 3$ pixel). BP_1 is a function of true rate constants only, which unlike K_1 are not affected by reduction in counts in the defined region due to limited resolution and partial volume effects. Hence, for an isolated structure, BP_1 should not show the pronounced bias associated with partial volume effects. However, spill over from adjacent structures with different kinetics, such as white matter into cortical regions, can introduce some bias in the estimates. Compared with the other parameters, the reliability of estimating BP_1 is relatively poor, with CV in some cases exceeding 80% and, hence, bias can also be expected due to the uncertainty in estimating this parameter. While some bias is still observed for BP_1 due to the reasons outlined above, it is less than the bias of the other parameters and there is a lack of systematic increase in bias of BP_1 with increasing FWHM.

TABLE III
EVALUATION SCORES OF ESTIMATED K_1 AND V_d

	Filter FWHM (pixel)						
Iterations	**0**	**3**	**4**	**5**	**6**	**7**	**8**
			5 subsets				
1	0	0	0	0	0	0	0
2	25	1	0	0	0	0	0
4	41	3	0	0	0	0	0
8	56	3	0	0	0	0	0
			10 subsets				
1	28	3	0	0	0	0	0
2	43	4	0	0	0	0	0
4	58	2	0	0	0	0	0
8	59	0	0	0	0	0	0
			20 subsets				
1	45	4	2	0	0	0	0
2	60	4	0	0	0	0	0
4	56	3	0	0	0	0	0
8	56	5	0	0	0	0	0
			30 subsets				
1	53	3	1	0	0	0	0
2	56	3	1	0	0	0	0
4	55	3	1	0	0	0	0
8	53	2	1	0	0	0	0
			40 subsets				
1	51	1	0	0	0	0	0
2	53	0	1	0	0	0	0
4	52	0	1	0	0	0	0
8	51	1	1	0	0	0	0
			60 subsets				
1	45	7	0	0	0	0	0
2	47	6	0	0	0	0	0
4	44	5	0	0	0	0	0
8	43	7	0	0	0	0	0

TABLE IV
EVALUATION SCORES OF ESTIMATED BP_1 AND BP_2

	Filter FWHM (pixel)						
Iterations	**0**	**3**	**4**	**5**	**6**	**7**	**8**
			5 subsets				
1	9	13	12	13	12	12	12
2	18	20	17	14	12	11	14
4	28	17	17	15	13	14	12
8	31	14	18	11	12	12	16
			10 subsets				
1	13	15	9	10	6	12	8
2	30	18	11	12	11	7	10
4	33	10	15	7	9	9	12
8	26	9	13	12	11	9	7
			20 subsets				
1	33	12	12	11	6	3	2
2	26	11	12	7	5	3	1
4	26	8	13	6	6	1	4
8	26	8	10	7	7	2	1
			30 subsets				
1	28	9	9	8	7	9	6
2	30	8	9	11	8	8	7
4	30	6	11	12	11	8	7
8	27	8	8	10	7	8	5
			40 subsets				
1	24	9	12	11	5	7	5
2	23	7	12	10	5	6	4
4	23	8	11	9	5	6	6
8	23	9	12	10	4	7	6
			60 subsets				
1	22	5	4	3	3	4	3
2	23	7	6	9	4	4	3
4	24	5	7	6	6	5	3
8	21	6	7	6	5	4	4

Fig. 6 plots the bias and CV as a function of reconstruction parameters (number of iterations and subsets) for estimates of K_1 and V_d in the thalamus without any post-reconstruction filtering. Low number of equivalent iterations, i.e., low number of subsets, combined with a low number of iterations, provides the least noise, but also the lowest resolution reconstruction and, hence, the largest bias. Particularly for V_d, low number of equivalent iteration does have a positive effect on CV. However, CV is quite low ($<3\%$) for all reconstruction parameter combinations and the small gain in CV is outweighed by the increase in bias. CV of K_1 is insensitive to the reconstruction parameters and $<7\%$ for all reconstructions of this parameter except one point with a spuriously elevated CV of 12.5%. The data suggest that an equivalent number of at least 40 iterations should be used based on bias considerations.

B. The Overall Evaluation Scores

The scores derived from the bias versus CV plots (see Fig. 2) are given in Table III for K_1 and V_d and in Table IV for BP_1 and BP_2. The maximum score for any filter and reconstruction parameter combination obtainable is 60 (3 regions, 10 noise levels, including noiseless data, and 2 parameters for each table). Based on these scores, reconstructions without filtering provided the best results for all reconstructions. This was quite clear cut for K_1 and V_d, but less pronounced for the binding potentials, as increased bias with increasing FWHM was not observed for BP_1 (see Figs. 4 and 5). Overall, the reconstructions that provided an equivalent number of 40 normal ML-EM iterations (i.e., 40 subsets and one iteration, 20 subsets and two iterations, 10 subsets and four iterations, five subsets and eight iterations) scored best. However, the exact reconstruction parameters do not appear to be critical. The parameter estimation only suffered from high noise at relatively high equivalent number of iterations (e.g., 40 subsets, four iterations). Conversely, at a low number of iterations (e.g., 10 subsets, one iteration) bias due to partial volume effect becomes pronounced. The overall evaluation for all the parameters of interest thus suggest that the noise control using the moderate number of 40 effective iterations and no post-reconstruction filtering provided the best tradeoff between bias and reliability.

C. Comparison Between Conventional and Bootstrap Monte Carlo Simulations

Table V lists the mean SDs and CVs estimated with Bootstrap and conventional MC of the parameters of interest for all

TABLE V
MEAN VALUES OF SD AND CV FOR BOOTSTRAP AND CONVENTIONAL MONTE CARLO SIMULATIONS FOR THE THREE VOLUMES OF INTERESTS AT NINE NOISE LEVELS (27 POINTS)

	K_1	V_d	BP_1	BP_2
Mean SD BMC	0.008±0.003	0.101±0.103	0.577±0.719	0.477±0.331
Mean SD CMC	0.007±0.003	0.082±0.096	0.642±0.897	0.493±0.431
Mean CV BMC (%)	3.0±1.1	0.6±0.4	24.9±15.7	6.1±2.0
Mean CV CMC (%)	2.6±1.2	0.5±0.4	24.1±21.6	5.5±1.9

BMC – Bootstrap Monte Carlo Technique
CMC – Conventional Monte Carlo Technique

VOIs and noise levels used for the comparisons. Good agreement is found between the SD and CV estimates obtained with Bootstrap and conventional MC techniques, vindicating taking advantage of the Bootstrap MC's substantial reduction in computation time.

D. Results With Resolution Recovery

Table VI compares the percentage bias from reconstructions with resolution recovery with bias obtained without resolution recovery for noise30. For K_1 and V_d, resolution recovery reduces the underestimation of the parameters observed without resolution recovery. The effect is most pronounced in the thalamus. A similar trend was also observed for BP_2, except in the cerebellum, where there was an increase in the overestimation of the parameter. BP_1 showed a slight reduction with resolution recovery of the overestimation observed without resolution recovery in all three regions.

CVs with resolution recovery were very similar to those without resolution recovery and were $<10\%$ for all the parameters of interests except BP_1. Although some CVs of BP_1 exceeded 80%, there was again little difference in reliability between reconstructions with and without resolution recovery for this parameter. Similar results for bias and CV were also observed at the other eight noise levels and the noise free data.

IV. DISCUSSION

While absolute physiological parameter estimation is well established in PET, it has only recently attracted attention in SPECT. Compared to PET, SPECT suffers from poorer resolution and decreased sensitivity, giving rise to more pronounced bias due to partial volume effects and high-noise levels in the image. Noise in the image can potentially be reduced with appropriate filtering or by reducing the effective number of iterations of the OS-EM reconstruction algorithm, but at the potential expense of degraded resolution and increased bias due to partial volume effects. In this study, we investigated the effect of reconstruction parameters and filtering on kinetic parameter bias and reliability for dynamic SPECT at varying noise levels.

To provide realistic simulated data, high-count Monte Carlo simulations of individual brain structures of a mathematical brain phantom were performed. Once projections of structures have been simulated, these can be combined into dynamic frames for any arbitrary tracer kinetics and noise level, without having to repeat any of the computationally intensive Monte Carlo simulations. For this study we elected to use the kinetics of the 5-[^{123}I]-iodo-A-85380, which had previously been studied in our institution [22], [23]. This tracer is fairly typical of the relatively slow kinetics observed with SPECT tracers. Simulating dynamic projection data allowed Poisson noise to be added to the projection data. This allowed the effect of the reconstruction, attenuation and scatter to be included in the simulations and evaluation and avoided the question of appropriate noise model and magnitude typically arising if noise is added to simulated dynamic curves or reconstructed image slice data.

As expected, bias increased with increasing filter FWHM and this effect was more pronounced for structures more affected by partial volume effect (thalamus and frontal cortex) than the larger, more homogenous cerebellum. Deriving TTACs from volumes of interest encompassing the structures provides spatial averaging of data with reduced noise compared to individual voxels, which may at least partially explain the lack of improvement in fit reliability with increased spatial filtering, which effectively is a form of spatial averaging (weighted) of the data. Increased spatial filtering will also increase spill-over between structures and, hence, curves derived from particular volumes of interest will contain a mixture of kinetics from different structures, and contamination from adjacent structures will increase with increasing filter FWHM, which may decrease the reliability of the estimated parameters. There was no systematic trend between bias and noise level. This suggests that the variation in bias between different noise levels is due to the uncertainty in estimating the parameters and slight differences in curve shape due to noise for the data sets, rather than systematic, noise level related bias.

Inclusion of resolution recovery in the OS-EM reconstruction has the potential of reducing partial volume effects. Less underestimation of K_1, V_d, and BP_2 was indeed observed with resolution recovery. However, resolution recovery was unable to completely recover the signal for small and thin structures like the thalamus and frontal cortex. Particularly for the frontal cortex, the improvement in bias was only modest. Convergence is significantly slower with resolution recovery, which increased reconstruction time by at least a factor of 20. Other methods for correcting for partial volume, such as techniques based on anatomical imaging [29], [30] or kinetic model based methods [31], [32] may perhaps be more successful in reducing bias, but are beyond the scope of this paper.

Due to interaction and high correlation between individual micro rate constants (k_2, k_3, k_4), the CV of these parameters was very high and reliability was poor. As in this case, the individual rate constants are usually of less interest and macro parameters related to physiological processes are more important. In this case K_1 gives an indication of tracer delivery and the macro parameters related to receptor binding (V_d, binding potentials) were of primary interest [22], [27], [28], [33] and, hence, investigation concentrated on these, rather than the individual rate constants. Fortunately, the reliability of the parameters of interest estimates is acceptable, even when the CVs of individual rate constants are very high.

TABLE VI
PERCENTAGE BIAS FOR PARAMETERS OF INTERESTS WITH AND WITHOUT RESOLUTION RECOVERY AT A MODERATE NOISE LEVEL FOR CEREBELLUM, FRONTAL CORTEX, AND THALAMUS

K_1			V_d			BP_1			BP_2		
NR	WR1	WR2	NR	WR1	WR2	NR	WR1	WR2	NR	WR1	WR2
cerebellum											
-4.3	5.0	4.1	-5.6	2.2	1.6	16.7	10.5	8.3	2.4	7.9	5.8
frontal cortex											
-43.7	-33.9	-31.5	-44.4	-35.7	-33.4	15.9	9.6	12.3	-40.9	-32.5	-29.4
thalamus											
-27.1	-19.2	-10.1	-34.5	-13.8	-4.0	28.7	21.4	26.3	-31.7	-10.4	0.6

NR – without resolution recovery and with 20 subsets and 2 iterations
WR1 – with resolution recovery and with 40 subsets and 10 iterations
WR2 – with resolution recovery and with 40 subsets and 20 iterations

The reliability of the parameter estimates can be directly derived from the fit of the parameters [24]. However, this only provides an indication of the CV of the parameters fitted, and not of the derived macro parameters, unless the fit is reformulated in terms of the macro parameters. In this case, the fitting equation would have had to be reformulated and applied separately for estimating CV of V_d,, BP_1, and BP_2. Bootstrap Monte Carlo technique avoided the need for reformulating the fit equation, with the potential for affecting results, while allowing CVs of both the micro and derived macro parameters to be estimated. The main disadvantage of Bootstrap Monte Carlo technique is increased computation time (100 fits to each TTAC in this case), which takes approximately 2 h on a Dell Dimension-4300 PC (1.5 GHz CPU, 512 MB of memory) including one reconstruction. However, it is significantly faster than conventional Monte Carlo simulations, which in this case would have taken 150 h to achieve 100 iterations of projection generation and reconstruction. Conventional Monte Carlo simulations were carried out for one reconstruction parameter set (20 subsets, two iterations) at all noise levels. This showed good agreement for estimates of SD and CV between conventional and bootstrap Monte Carlo simulations (Table V).

While the Bootstrap Monte Carlo technique is more time consuming than estimating the parameters' SD and CV directly with the fitting routine, the final parameter estimates are the mean of the parameter estimated at each Bootstrap Monte Carlo iterations. This should provide an improved estimate of the parameters compared to just a single fit to the data, as the standard error of the mean from the Bootstrap Monte Carlo estimates can be expected to be lower than the standard deviation of individual parameter fits returned by the fitting routine on convergence.

Rate constants k_2, k_3, and k_4 are not affected by partial volume effects and only K_1 and derived parameters containing K_1 are sensitive to partial volume effects. Thus, V_d (1) and BP_2 (3) are expected to be affected by partial volume effects, while BP_1 (2) should be relatively immune to resolution effects. This is indeed observed (see Figs. 4 and 5). However, reliability of estimating BP_1 is relatively poor and interaction between the fitted parameters as well as spill-over from regions with different kinetics may have resulted in some of the high biases observed for BP_1 for some reconstructions. BP_1 was the only parameter investigated which potentially benefited from post-reconstruction filtering.

V. CONCLUSION

We have investigated the effect of reconstruction and filtering on dynamic SPECT kinetic parameter estimation bias and reliability. Dynamic projection data were generated from high-count Monte Carlo simulations of a mathematical human brain phantom. Poisson noise at 10 different noise levels based on experimental count levels was added to the scaled projection. It was found that post-reconstruction filtering was not effective in improving reliability, but adversely affected bias, particularly in areas most affected by partial volume effect. Noise control using a moderate number of 40 effective iterations and no filtering provided the best tradeoff between bias and reliability. Further investigations are warranted such as incorporation of regularization into the reconstruction and clustering to improve reliability of estimates, particularly for high-noise studies, while not adversely affecting the bias of the estimated parameters [34], [35]. Incorporation of resolution recovery was only moderately successful in reducing bias and exploration of other partial volume correction techniques is warranted to reduce bias.

ACKNOWLEDGMENT

The authors are grateful to Dr. I. G. Zubal, Department of Diagnostic Radiology, Yale School of Medicine, for his generosity in supplying the mathematical brain phantom.

REFERENCES

[1] M. S. Rosenthal, J. Cullom, W. Hawkins, S. C. Moore, B. M. W. Tsui, and M. Yester, "Quantitative SPECT imaging: A review and recommendations by the focus committee of the society of nuclear medicine computer and instrumentation council," *J. Nucl. Med.*, vol. 36, pp. 1489–1513, Aug. 1995.

[2] H. Zaidi, "Quantitative SPECT: Recent developments in detector response, attenuation and scatter compensation techniques," *Phys. Medica.*, vol. 12, pp. 101–117, Jul.–Sep. 1996.

[3] K. Van Laere, M. Koole, I. Lemahieu, and R. Dierckx, "Image filtering in single-photon emission computed tomography: Principles and applications," *Comput. Med. Imaging Graph.*, vol. 25, pp. 127–133, Mar.–Apr. 2001.

[4] R. E. Carson, Y. C. Yan, B. A. Chodkowski, T. K. Yap, and M. E. Daube-Witherspoon, "Precision and accuracy of regional radioactivity quantitation using the maximum likelihood EM reconstruction algorithm," *IEEE Trans. Med. Imag.*, vol. 13, no. 3, pp. 526–537, Sep. 1994.

[5] K. Lange and R. Carson, "EM Reconstruction algorithms for emission and transmission tomography," *J. Comput. Assisted Tomography*, vol. 8, pp. 306–316, Apr. 1984.

[6] B. M. W. Tsui, G. T. Gullberg, E. R. Edgerton, J. G. Ballard, J. R. Perry, W. H. McCartney, and J. Berg, "Correction of nonuniform attenuation in cardiac SPECT imaging," *J. Nucl. Med.*, vol. 30, pp. 497–507, Apr. 1989.

[7] Y. Narita, S. Eberl, H. Iida, B. F. Hutton, M. Braun, T. Nakamura, and G. Bautovich, "Monte Carlo and experimental evaluation of accuracy and noise properties of two scatter correction methods for SPECT," *Phys. Med. Biol.*, vol. 41, pp. 2481–2496, Nov. 1996.

[8] L. A. Shepp and Y. Vardi, "Maximum likelihood reconstruction for emission tomography," *IEEE Trans. Med. Imag.*, vol. MI-1, no. 2, pp. 113–122, Oct. 1982.

[9] H. H. Barrett, D. W. Wilson, and B. M. W. Tsui, "Noise properties of the EM algorithm: I. Theory," *Phys. Med. Biol.*, vol. 39, pp. 833–846, May 1994.

[10] H. M. Hudson and R. S. Larkin, "Accelerated image reconstruction using ordered subsets of projection data," *IEEE Trans. Med. Imag.*, vol. 13, no. 4, pp. 601–609, Dec. 1994.

[11] D. S. Lalush, S. S. Karimi, and B. M. W. Tsui, "Convergence and resolution recovery of block-iterative EM algorithms modeling 3D detector response in SPECT," in *Proc. IEEE Nuclear Science Symp. Medical Imaging*, Anaheim, CA, 1996, pp. 1648–1622.

[12] C. Kamphuis, F. J. Beekman, and M. A. Viergever, "Evaluation of OS-EM vs. ML-EM for 1D, 2D, and fully 3D SPECT reconstruction," *IEEE Trans. Nucl. Sci.*, vol. 43, no. 3, pp. 2018–2024, Jun. 1996.

[13] J. M. Links, R. W. Jeremy, S. M. Dyer, T. L. Frank, and L. C. Becker, "Wiener filtering improves quantification of regional myocardial perfusion with thallium-201 SPECT," *J. Nucl. Med.*, vol. 31, pp. 1230–1236, Jul. 1990.

[14] M. A. King, S. J. Glick, and B. C. Penney, "Activity quantitation in SPECT: A comparison of three attenuation correction methods in combination with pre-reconstruction restoration filtering," *IEEE Trans. Nucl. Sci.*, vol. 38, no. 2, pp. 755–760, Apr. 1991.

[15] B. M. W. Tsui, X. D. Zhao, Z. J. Cao, and E. C. Frey, "Reconstruction methods for quantitative brain SPECT," *IEEE Trans. Nucl. Sci.*, vol. 40, no. 2, pp. 214–220, Apr. 1993.

[16] R. G. Wells, P. H. Simkin, P. F. Judy, M. A. King, P. H. Pretorius, H. C. Gifford, and P. Schneider, "Maximizing the detection and localization of Ga-67 tumors in thoracic SPECT MLEM(OSEM) reconstructions," *IEEE Trans. Nucl. Sci.*, vol. 46, no. 4, pp. 1191–1198, Aug. 1999.

[17] E. T. P. Slijpen and F. J. Beekman, "Comparison of post-filtering and filtering between iterations for SPECT reconstruction," *IEEE Trans. Nucl. Sci.*, vol. 46, no. 6, pp. 2233–2238, Dec. 1999.

[18] B. F. Hutton and Y. H. Lau, "Application of distance-dependent resolution compensation and post-reconstruction filtering for myocardial SPECT," *Phys. Med. Biol.*, vol. 43, pp. 1679–1693, Jun. 1998.

[19] F. J. Beekman, E. T. P. Slijpen, and W. J. Niessen, "Selection of task-dependent diffusion filters for the post-processing of SPECT images," *Phys. Med. Biol.*, vol. 43, pp. 1713–1730, Jun. 1998.

[20] I. G. Zubal, C. R. Harrell, E. O. Smith, Z. Rattner, G. Gindi, and P. B. Hoffer, "Computerized 3-dimensional segmented human anatomy," *Med. Phys.*, vol. 21, pp. 299–302, Feb. 1994.

[21] T. K. Lewellen, R. L. Harrison, and S. Vannoy, "The simset program," in *Monte Carlo Calculations in Nuclear Medicine, Medical Science Series*, M. Ljungberg, S. E. Strand, and M. A. King, Eds. Bristol, U.K.: Institute of Physics, 1998, pp. 77–92.

[22] M. Kassiou, S. Eberl, S. R. Meikle, A. Birrell, C. Constable, M. J. Fulham, D. F. Wong, and J. L. Musachio, "In vivo imaging of nicotinic receptor upregulation following chronic (-)-nicotine treatment in baboon using SPECT," *Nucl. Med. Biol.*, vol. 28, pp. 165–175, Feb. 2001.

[23] K. P. Wong, S. Eberl, D. Feng, M. Kassiou, and M. J. Fulham, "Kinetic modeling of nicotinic acetylcholine receptors with 5-[^{123}I]iodo-A-85 380 and dynamic single-photon emission computed tomography," in *Proc. Int. Federation Automatic Control (IFAC) 15th World Congress*, Barcelona, Spain, Jul. 21–26, 2002.

[24] W. H. Press, S. A. Teukolsky, W. T. Vetterling, and B. P. Flannery, *Numerical Recipes in C: The Art of Scientific Computing*, 2nd ed. Cambridge, U.K.: Cambridge Univ. Press, 1992, pp. 656–706.

[25] C. H. Lau, S. Eberl, D. Feng, H. Iida, P. K. Lun, W. C. Siu, Y. Tamura, G. J. Bautovich, and Y. Ono, "Optimized acquisition time and image sampling for dynamic SPECT of Tl-201," *IEEE Trans. Med. Imag.*, vol. 17, no. 3, pp. 334–343, Jun. 1998.

[26] X. Li and D. Feng, "Toward the reduction of dynamic image data in positron emission tomography studies," *Comput. Meth. Prog. Biomed.*, vol. 53, pp. 71–80, Jun. 1997.

[27] M. A. Mintun, M. E. Raichle, M. R. Kilbourn, G. F. Wooten, and M. J. Welch, "A quantitative model for the in vivo assessment of drug binding sites with positron emission tomography," *Ann. Neurol.*, vol. 15, pp. 217–227, Mar. 1984.

[28] M. Laruelle, E. Wallace, J. Seibyl, R. Baldwin, Y. Zea-Ponce, S. Zoghbi, J. Neumeyer, D. S. Charney, P. B. Hoffer, and R. B. Innis, "Graphical, kinetic, and equilibrium analyzes of in-vivo I-123 beta-cit binding to dopamine transporters in healthy human subjects," *J. Cereb. Blood Flow Metab.*, vol. 14, pp. 982–994, Nov. 1994.

[29] H. W. Müller-Gärner, J. M. Links, J. L. Prince, R. N. Bryan, E. McVeigh, J. P. Leal, C. Davatzikos, and J. J. Frost, "Measurement of radiotracer concentration in brain gray matter using positron emission tomography: MRI-based correction for partial volume effects," *J. Cereb. Blood Flow Metab.*, vol. 12, pp. 571–583, Jul. 1992.

[30] K. Kalki, S. C. Blankespoor, J. K. Brown, B. H. Hasegawa, M. W. Dae, M. Chin, and C. Stillson, "Myocardial perfusion imaging with a combined x-ray CT and SPECT system," *J. Nucl. Med.*, vol. 38, pp. 1535–1540, Oct. 1997.

[31] H. Iida, I. Kanno, A. Takahashi, S. Miura, M. Murakami, K. Takahashi, Y. Ono, F. Shishido, A. Inugami, N. Tomura, S. Higano, H. Fujita, H. Sasaki, H. Nakamichi, S. Mizusawa, Y. Kondo, and K. Uemura, "Measurement of absolute myocardial blood flow with $H_2^{15}O$ and dynamic positron-emission tomography. Strategy for quantification in relation to the partial-volume effect," *Circulation*, vol. 78, pp. 104–115, Jul. 1988.

[32] L. I. Araujo, A. A. Lammertsma, C. G. Rhodes, E. O. McFalls, H. Iida, E. Rechavia, A. Galassi, R. DeSilva, T. Jones, and A. Maseri, "Noninvasive quantification of regional myocardial blood flow in coronary artery disease with oxygen-15-labeled carbon dioxide inhalation and positron emission tomography," *Circulation*, vol. 83, pp. 875–885, Mar. 1991.

[33] A. Abidargham, M. Laruelle, J. Seibyl, Z. Rattner, R. M. Baldwin, S. S. Zoghbi, Y. Zeaponce, J. D. Bremner, T. M. Hyde, D. S. Charney, P. B. Hoffer, and R. B. Innis, "SPECT Measurement of benzodiazepine receptors in human brain with iodine-123-iomazenil-kinetic and equilibrium paradigms," *J. Nucl. Med.*, vol. 35, pp. 228–238, Feb. 1994.

[34] D. Ho, D. Feng, and K. Chen, "Dynamic image data compression in spatial and temporal domains: Theory and algorithm," *IEEE Trans. Inf. Technol. Biomed.*, vol. 1, no. 4, pp. 219–228, Dec. 1997.

[35] D. J. Kadrmas, E. V. R. DiBella, R. H. Huesman, and G. T. Gullberg, "Analytical propagation of errors in dynamic SPECT: estimators, degrading factors, bias, and noise," *Phys. Med. Biol.*, vol. 44, pp. 1997–2014, Aug. 1999.